Development of a Cast Modular Connector for Seismic-Resistant Steel Moment Frames Part 2: Experimental Verification

ALI SUMER, ROBERT B. FLEISCHMAN, and NATHAN J. PALMER

A companion paper (Sumer, Fleischman, and Hoskisson, 2007) describes the analytical development of a cast modular connector (MC) for seismic-resistant steel moment frames. The MC is a field-bolted connector between the beam flange and column, and is therefore identical in position and similar in form to structural tee (WT) sections (AISC, 2001) used in the traditional semi- or fully-rigid bolted T-stub connections (Swanson and Leon, 2000). The MC is intended to serve as the special energy-dissipating detail. The MC development involved analytical research examining the monotonic response of isolated connectors. The result is a second-generation MC (Beta) prototype design. The design is described in terms of optimum geometric properties and includes a set of design expressions for connector stiffness, strength and ductility.

This paper describes the prototyping and experimental verification of the MC Beta prototype, including an examination of the connector's cyclic performance. Industry partners from AISC and SFSA (Steel Founder's Society of America) worked with the research team to guide and ultimately perform the prototype casting and fabrication. The MC Beta prototype was cast at approximately half-scale. The experimental verification of the MC Beta prototype design, consistent with the analytical development, was performed on isolated connectors. Monotonic and cyclic load tests performed on isolated MCs and WT sections of similar strength and stiffness revealed the MC Beta prototype as clearly superior to its traditional (WT) counterpart.

Ali Sumer is research assistant, department of civil and engineering mechanics, University of Arizona, Tucson, AZ.

Robert B. Fleischman is assistant professor, department of civil and engineering mechanics, University of Arizona, Tucson, AZ.

Nathan J. Palmer is engineer I, grade P-08, Parsons Brinckerhoff Quade & Douglas, Inc., Tempe, AZ.

Subsequent developmental steps will include an analytical examination and full-scale experimental evaluation of beam-to-column joints containing the MC using accepted testing protocols (AISC, 2005); and the development of a design procedure for frames using the MC. These subsequent developmental steps are briefly summarized at the end of the paper (see Future Work).

MC BETA PROTOTYPE DESIGN

The MC Beta prototype design is briefly summarized (Sumer et al., 2007). Figure 1 shows a schematic of the MC Beta prototype. The intent of the MC design is to provide highly ductile and reliable performance through: (1) a series of variable cross-section "arm" elements that produce a plastic zone distributed along the entire length of the element thereby reducing the intensity of strain concentrations; and (2) end-regions connected by a base that create a set of self-equilibrating forces, thereby eliminating prying on the bolts.

Tables 1a and 1b summarize the relationships used to configure the MC Beta prototype. Expressions derived in the companion paper (Sumer et al., 2007) for optimum geometry appear in Table 1a. As can be seen, most aspects of the MC geometry can be related back to arm length, *L*. Optimum arm geometry (see Figure 1a) is given in terms of ratios directly related to *L*. Optimum end region geometry (see Figure 1a),

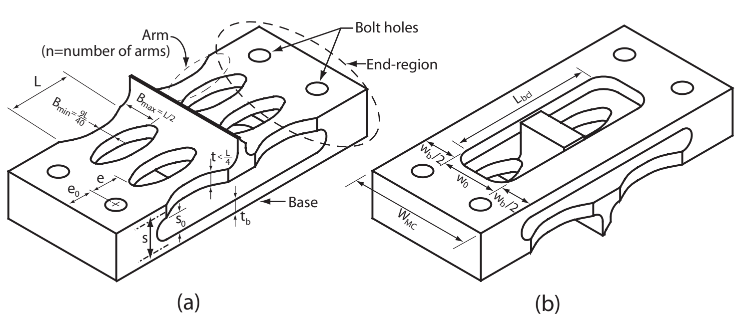

Fig. 1. MC Beta configuration: (a) isometric view; (b) underside.

Table 1a. MC Beta Design: Optimum Geometry		
Segment	**Equations**	**Equation Number**
Arm	$B_{max} = L/2$	(T1)
	$B_{min} = 9L/40$	(T2)
	$t < L/4$	(T3)
End-Region	$2s - t = \left(1.5\frac{t}{L} + 1\right)e$	(T4)
	$e_0 = s - (t + t_b)/2$	(T5)
Base[a]	$W_{MC} \cong 1.2\ nL/4$	(T6)
	$L_{bcl} \cong 2.5L$	(T7)
	$w_b \cong 0.16nL$	(T8)
	$t_b > \sqrt[3]{4.25C_{t2}L^2F_u/E}$	(T9a)
	$t_b > 0.52C_{t2}F_u/F_y$	(T9b)

[a] $C_{t2} = \dfrac{2t}{\sqrt{4+\sqrt{t}}}$

Table 1b. MC Beta Design: Prototyping		
	Equations	**Equation Number**
Castability	$t > 0.75$	(T10)
	$t_b > 0.75$	(T11)
	$S_0 > 0.75$	(T12)
	$W_0 \cong 0.43\ W_{MC}$	(T13)
Ductility	$L > d_{bm}/6.5$	(T14)

expressed as a ratio between the bolt-to-arm eccentricity, e, and the arm-base separation, s, is based on arm length, L, and thickness, t. Base dimensions (see Figure 1b) are related to the number, n, and size (in terms of L) of the arms.

The optimum arm geometry produces a highly ductile response, provided that the arm elements possess sufficient length. The optimum end region permit the use of longer arm elements by eliminating significant demands on the bolt, including bolt prying and a catenary-action induced shear failure mode (Sumer et al., 2007). Fasteners can simply be sized for the direct flange force. The base region must carry high compressive forces and thus the base thickness, t_b, is sized to prevent base buckling and yielding (see Table 1a).

Design expressions for the properties of the MC Beta prototype were derived in the companion paper (Sumer et al., 2007). These expressions are indicated on the connector load-deflection response schematic shown in Figure 2, and include connector stiffness, K_i, yield strength, P_y, ultimate strength, P_u, and the so-called "stability point" deflection, Δ_u. The expressions are primarily functions of the independent variable L, and are converted from "arm" properties to "connector" properties through scaling by the number of arms, n (refer to Figure 1a). For generality, the thickness parameter, t, also appears in expressions because t need not exactly equal $L/4$. The bolt design is also indicated on the schematic, based on capacity design concepts.

Expressions determined in the prototyping, as described in this paper, appear in Table 1b. These expressions pertain to castability (see "Castability Considerations") and the selection of the arm length, L, for ductility. The latter requires consideration of the full connection response, in which the "connector" properties shown in Figure 2 are transformed into "connection" properties (see "Determining an Appropriate Arm Length").

CASTABILITY CONSIDERATIONS

A major challenge in developing the MC is to create a configuration that meets the seismic performance requirements and at the same time can be reliably cast. Toward this goal, industry partners from SFSA collaborated closely in the development of the MC Beta prototype design. Certain geometries that are desirable for the seismic performance of the MC are not ideal from a castability standpoint and thus require quality control to ensure a sound casting. In this section, the castability issues specific to the MC geometry and the eventual solutions that created a viable prototype design are described in detail.

Casting Quality Control

Traditionally, quality control measures occur after a casting has already been created, including mechanical testing, chemical spectrography, and nondestructive evaluation. For this research, recent advances in computer simulation of the casting solidification process provided the opportunity to perform quality control prior to casting. Industry partners and university researchers were able to rapidly arrive at feasible geometries by iterating between structural and thermodynamic/fluid flow finite element analysis through the electronic exchange of three-dimensional solid geometry CAD files. Consider Figure 3a, a contour plot of shrinkage

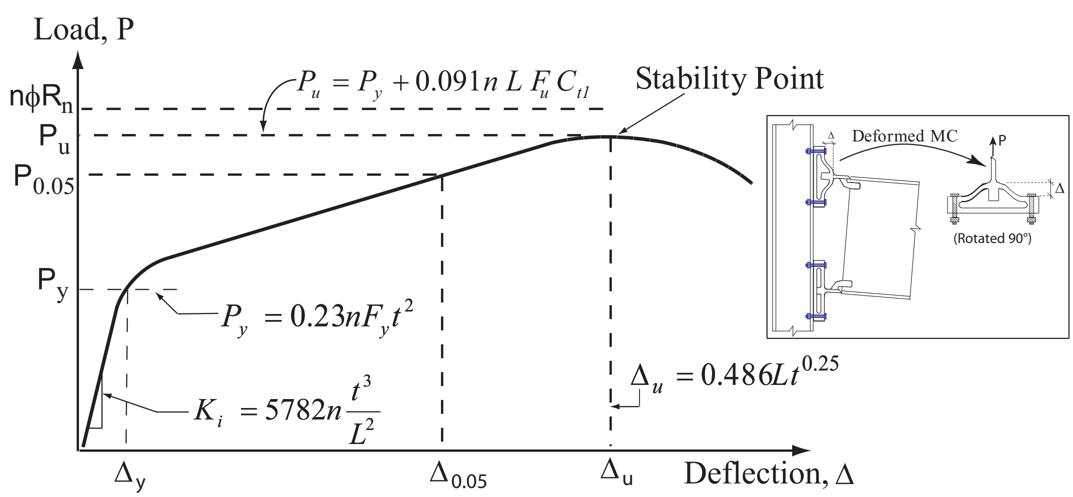

Fig. 2. Global parameters indicating design equations.

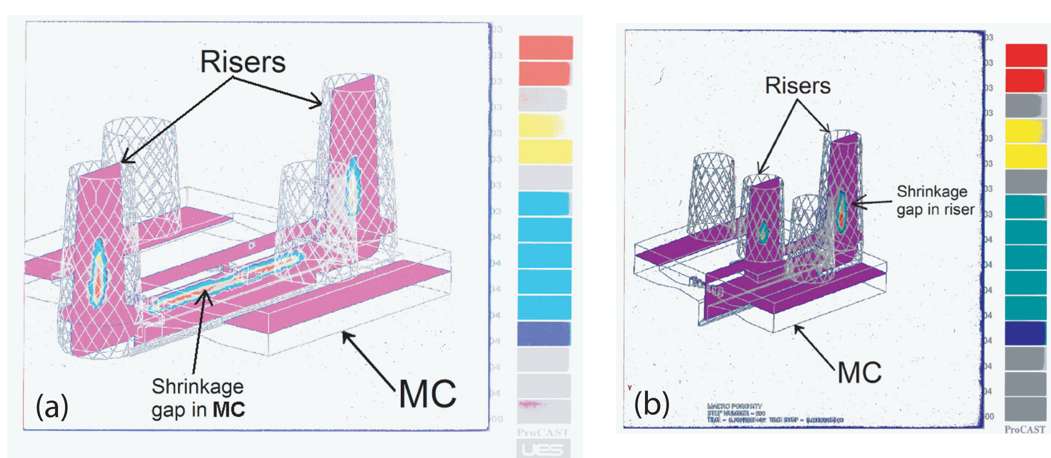

Fig. 3. Contour plots of shrinkage gaps from solidification analysis: (a) original riser layout; (b) modified layout.

gaps obtained from a solidification analysis of an early MC design. As seen, shrinkage voids occur in the cast piece, a clearly unacceptable outcome. A redesign of the gating (in other words, where molten metal enters the mold) and riser layout (gravity-driven liquid feed metal reservoirs within the mold) is shown in Figure 3b in which the shrinkage gaps occur outside the cast piece (in the risers). This process took a few days of computer time rather than the time and cost of pattern-making, forming molds, casting, and proof testing of test piece(s).

Castability Issues for the MC Prototype

Many castability issues are not solved simply by redesigning gates and risers; changes to the shape of the cast piece itself are often required. Recognizing these type of issues as a source of the poor performance of the Alpha prototype test (Sumer et al., 2007), SFSA identified an appropriate industry partner (SFSA member Varicast, Inc., now known as Vancouver Iron and Steel, Inc.) to collaborate more closely in developing a prototype design that is optimized based on both structural and castability requirements.

Working with Varicast, the research team was able to make several significant modifications for the MC Beta prototype (Varicast, 2002) and specify a new steel material (see next section). The challenge in the modifications to geometry is that satisfying the objectives of a structural and castable design often involves competing requirements. The Alpha prototype geometry is reproduced in Figure 4 to help illustrate this point in the discussions that follow, with regions associated with castability issues ("CI") indicated.

Consider first the "hourglass" shaped arm elements where thin-to-thick transitions are essential to accomplish the intended structural intent (see "CI #1" in Figure 4). Without any special attention, the smaller cross-section will tend to solidify first, cutting off the flow of molten steel to the surrounding regions, and increasing the chance of shrinkage gaps. Given the key role of these arm elements as reliable seismic energy dissipators at high ductility demand, it is clearly unacceptable for this portion of the casting to be susceptible to shrinkage gaps. However, since the small-to-large section transition is an essential part of the MC design, it also cannot be abandoned. Instead, the design requires subtle modifications in the MC shape itself to ensure the shrinkage gaps do not occur.

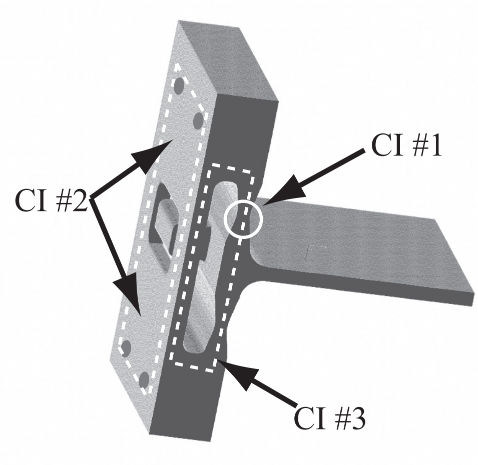

Fig. 4. Alpha prototype regions causing casting issues (CI).

Next consider the base detail, shown in Sumer et al. (2007) as the end-region alternative that provides the desired structural characteristics (see "CI #2" in Figure 4). The closed-section formed by joining each end-region by the base presents certain casting difficulties. First, it is relatively difficult to feed the entire base region with molten steel and riser placement is not straightforward. Secondly, analyses by Varicast anticipated "hot tears" (SFSA, 1995), an irregularly shaped fracture caused by hindered contraction in steep thermal gradient zones within the casting during solidification in the corners of a solid base.

Finally, bolt prying reduction has been shown to be dependent on the arm/base separation dimension, *s*, which is controlled by the size of the opening between the arm and the base (see "CI #3" in Figure 4). This cavity is formed through a sand core placed in the mold to create the internal opening. This core is entirely surrounded by molten steel during the casting process and requires sufficient volume to dissipate the required density of heat and resist buoyancy forces produced by the surrounding molten steel. An isolated core of insufficient volume will begin to degrade and/or float thus compromising the quality of the casting.

The aforementioned castability issues surrounding the Alpha prototype were eliminated by a number of modifications to the shape introduced in the MC Beta prototype (see Table 1b): (1) the single variable-thickness arm was replaced by a series of variable width arms (as shown in Figure 1a); (2) an opening matching the projection of the arms (L_{bcl}) and occupying slightly less than half the width ($w_0 = 0.43\ W_{MC}$) was provided in the previously solid base (as shown in Figure 1b); (3) a minimum wall thickness of 0.75 in. was specified for t, t_b; (4) a minimum opening between the arm and the base, $s_0 > 0.75$ in. (see Figure 1a), was specified to provide sufficient core thickness (Varicast, 2002); and, (5) the proportion of the MC comprising the end region was reduced (compare end regions in Figures 1a and 4). In total, these changes improve the molten steel feed; the arrangement is easier to feed with risers; the opening in the base prevents the "hot tear" condition; and, finally, the openings between the arms and in the base permit the outer portions of the mold to anchor the core, thus preventing buoyancy issues.

Table 2. Chemical Composition of MC Alpha and Beta Prototypes											
Prototype	C	Si	Mn	P	S	Cr	Ni	Mo	Cu	V	Al
Alpha	0.112	0.434	0.465	0.023	0.015	.055	0.016	0.009	–	–	0.06
Beta	0.15 (0.15 – 0.20)	0.42	0.42	0.01	0.01	0.02 (0.12 max)	0.01	0.01 (0.08 max)	0.03 (0.25 max)	0.00	0.04

In conjunction with a new steel material, these modifications will be shown to produce high quality castings (see "Experimental Results").

Cast Steel Material

A cast steel was selected once a viable cast configuration had been identified. As a special seismic detail in the structure, the performance requirements for the MC center on ductility, not strength. Recognizing this as an atypical requirement for cast material, readily available yet custom made steel was chosen for the MC Beta prototype rather than the direct use of an existing cast steel specification. The material is a mild steel similar to ASTM A915/A915M (ASTM, 2003) Grade SC 1020 produced in conjunction with a heat treatment process including normalizing and stress relieving (Varicast, 2002). Table 2 provides the chemical composition of this steel, and a comparison to the Dynamo steel used in the Alpha prototype (Eagle Alloy, 2000). The mechanical properties were taken from a separately cast double keel bar (a Y-shaped casting poured alongside the cast product for later machining into two tensile coupons) per ASTM A781/A781M (ASTM, 2004). These properties appear in Table 4 (see "Experimental Program, Test Specimens").

CREATING THE MC BETA PROTOTYPE

Sizing Criteria

The sizing of the MC Beta prototype is driven by the desire to perform a full-scale beam-to-column connection test under accepted loading protocols (AISC, 2005) in the next phase of the research. Accordingly, a target ultimate strength, P_u, of 500 kips was set for the MC Beta prototype, based on the following guidelines: (1) the 220-kip actuating capacity at the University of Arizona structures laboratory; (2) a one-sided test for typical dimensions of 13-ft floor-to-floor height and 30-ft bays; (3) a 33 in. beam available at the AISC industry partner; (4) the significant overstrength observed in the MC, in other words, the difference between the connection's yield strength, P_y, and ultimate strength, P_u; (5) appropriate factors of safety based on allowance for strength variances and the possible contribution to flexural strength from the web connection. Eight arms were chosen for the MC Beta Prototype in order to evaluate the castability of an MC with several openings.

Determining an Appropriate Arm Length

The selection of the MC arm length is driven by the design requirement that the stability point, Δ_u, occur beyond a useful connection rotational demand, θ_{use}, of 0.05 radian (Sumer et al., 2007). This (monotonic) value differs from the accepted cyclic ductility requirement of 0.04 radian (AISC, 2005) for reasons that will become apparent in a subsequent section, "Cyclic Response (Constant Amplitude)." Connector deflection can be related to connection rotation through a simple displacement transformation assuming rotation about the opposing flange (see Figure 5), rendering the stability point requirement as

$$\Delta_u > (\theta_{use}\, d_{bm}) \times F.O.S. \qquad (1)$$

Thus, the needed connector deformation capacity is a beam-depth dependent quantity. MC designs employ an arm thickness close to the allowable upper limit of $L/4$ in order to maximize strength and stiffness (Sumer et al., 2007) and to assist in castability. Thus an approximate expression for Δ_u

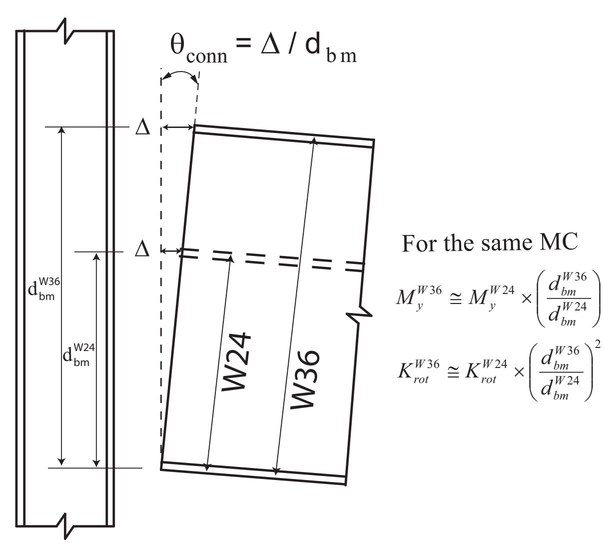

Fig. 5. Deformation under different beam depths.

Table 3. MC Beta Prototype Properties																	
	Arm-Related Parameters					MC Design Properties				Bolt Design				Base Design			
MC Beta Prototype	L in.	t in.	n	F_y ksi	F_u ksi	P_y kips	P_u kips	K_i kip/in.	Δ_u in.	n_b	Bolt Type	e in.	s in.	t_b in.	w_b in.	L_{bcl} in.	W_{MC} in.
Full-Scale	6.0	1.25	8	40	70	115	473	2510	3.08	8	1 in. A490	2.45	2.5	1.25	8.3	15	14.5
Scaled	4.3	0.78	6	40	70	34	143	890	1.96	4	⅞ in. A325	2.69	2.1	0.75	4.1	9.2	7.5

can be given entirely in terms of L by substituting $t = L/4$ into the design expression for Δ_u given in Figure 2,

$$\Delta_u = 0.344\, L^{5/4} \tag{2}$$

This expression for Δ_u can be inserted into Equation 1 in order to determine an appropriate arm depth,

$$L > 0.3\, d_{bm}^{\;4/5} \tag{3}$$

where a factor of safety of 1.5 is used in the design since the actual thickness can be lower than $L/4$ (unconservative). The linear relationship $L > d_{bm}/6.5$ provides a least-squares fit over typical steel beam depths and is used as the design expression for minimum required arm length (see Table 1b).

It will be advantageous from a standpoint of modularity to use a single size MC with several different beam depths (see "Guidelines for the Design of MCs"). Thus, the arm length chosen for a given MC should be based on the deepest beam anticipated in order for the design to provide deformation capacity over the range of possible depths (refer to Figure 5). On the basis of a maximum possible beam depth of 40 in., the MC Beta prototype was provided a 6-in. leg to satisfy Equation 3.

MC Beta Prototype

The resulting geometry and design properties for the MC Beta Prototype are shown in the "Full-Scale" row of Table 3. The MC end region is configured once the arm and base thickness are established. The smallest allowable values of e and s are desirable for fit-up. These values are determined by first calculating the minimum arm/base separation, s, for castability, in other words, $s = s_0 + (t + t_b)/2$ where $s_0 = 0.9$ was chosen for the Beta prototype and the base thickness is calculated from Equations T10a and T10b of Table 1a with a factor of safety of 1.25 used in the design. The bolt-to-arm eccentricity, e, can then be determined from Equation T4 in Table 1a.

The MC Beta Prototype will be: (1) evaluated at full-scale in full beam-to-column connections under the AISC protocol; and, (2) referenced to a joint in a prototype structure for future system evaluations (see "Future Work"). For the stage in the development of the MC reported in this paper, namely the verification of the form of the connector itself, a scaled version is used as described next.

Scaled MC Beta Prototype

The analytically developed MC Beta prototype form is experimentally verified through tests of the isolated connector. These tests are performed rapidly as direct pull tests. Such tests provide boundary conditions matching the analyses, thus providing direct experimental verification. The tensile machine capacity at the University of Arizona laboratory is 200 kips. For this reason, a scaled version of the MC Beta prototype was developed whose strength resides within this capacity.

These tests also permit a direct comparison of the MC to a traditional WT. Accordingly, the scaling was selected such that MCs and WTs of the same nominal strength and stiffness could be compared. The dimensions of the scaled MC Beta prototype and the WT are shown in Figure 6a and 6b respectively. The following procedure was used in the scaling: (1) the rules governing optimum arm geometry and end configuration were maintained; (2) arm length was reduced to match the longest possible effective gage of a WT (in other words, 4.3 in.); (3) the length-to-thickness ratio was adjusted in the scaling to produce the same nominal strength in the MC and the WT, while still meeting the required limiting ratio L/t of 4; and, (4) all dimensions were maintained within the castable range as discussed in the previous section, in particular, the minimum thickness required for castability. It is noted that meeting this last requirement led to a reduction in the number of arms in the scaled connector (8 to 6).

The scaled arm geometry and resulting design properties appear in the "Scaled" row of Table 3. Because of the multiple constraints, a direct scaling factor on dimension does not exist; however, arm length and thickness are both between one-half and three-quarters scale, producing a 2.5 fold reduction in nominal yield strength for a single arm.

The end region geometric parameters and the bolts selected are also shown in Table 3. Using the scaled MC prototype geometry, Equation T4 from Table 1a becomes

$$(e + 0.654)/s = 1.594 \tag{4}$$

with the end region geometry selected as described in the previous section, except in this case s_0 = 1.32 in. It is noted that in order to verify the optimal end region geometry, tests were performed with dimensions that did and did not satisfy Equation 4.

The eventual full-scale testing of the MC Beta prototype under the AISC protocol (AISC, 2005) will occur on a W33 beam. An implied beam depth for the scaled prototype is estimated by the ratio of arm lengths (33 in. × 4.3 in./6 in. = 23.7 in.). Thus the loading protocol for the scaled MC Beta prototype is referenced to a W24 beam in order to maintain similar connector deformation demand at a given connection rotation.

ANALYTICAL PREDICTION

Two-dimensional finite element analyses were used to predict the performance of the MC and WT specimens. The basic analytical model from the MC development phase was used for these predictions. New versions modified for cyclic behavior were also evaluated. The experiments reported in this paper verify these analytical models.

Basic Analytical Model

The basic analytical model was created using the commercial software package ANSYS (2003) and is described in detail in Sumer et al. (2007). To make the experimental predictions, data from uniaxial tension tests of the cast steel were used to construct the material model. The stress-strain response from these tests was reproduced as multilinear curves and converted to true stress-strain for large deflection analyses. A multilinear kinematic (MKIN) hardening material model was used.

The basic analytical material model will be shown to produce excellent local agreement in the monotonic experiments up to high plastic strain demand (20% strain). Further, the adequacy of the technique used to predict deformation capacity of the MC, that is the assumption of ductile crack formation at the maximum uniaxial (true) strain value of 0.285 (Fleischman and Sumer, 2006) is also confirmed in the experiments. The successful predictions point to the potential for using analytical models in the development of the family of MCs for off-the-shelf use (see "Future Work"). However, for analytical modeling to be fully useful in engineering future designs of the MC, the cyclic performance must also be adequately predicted. The MKIN model has difficulty in accurately modeling this behavior.

Analytical Models for Cyclic Response

To adequately predict cyclic performance of the MC, analytical models must: (1) accurately track cumulative plastic strain for low cycle fatigue life predictions under cyclic ductility demands; and (2) capture the second order effects exhibited as the elongated arm is cycled back in compression. Two alternatives to the MKIN material model are evaluated as cyclic strain models: an isotropic hardening model (MISO) and a combined rule (isotropic and kinematic) (Dar-

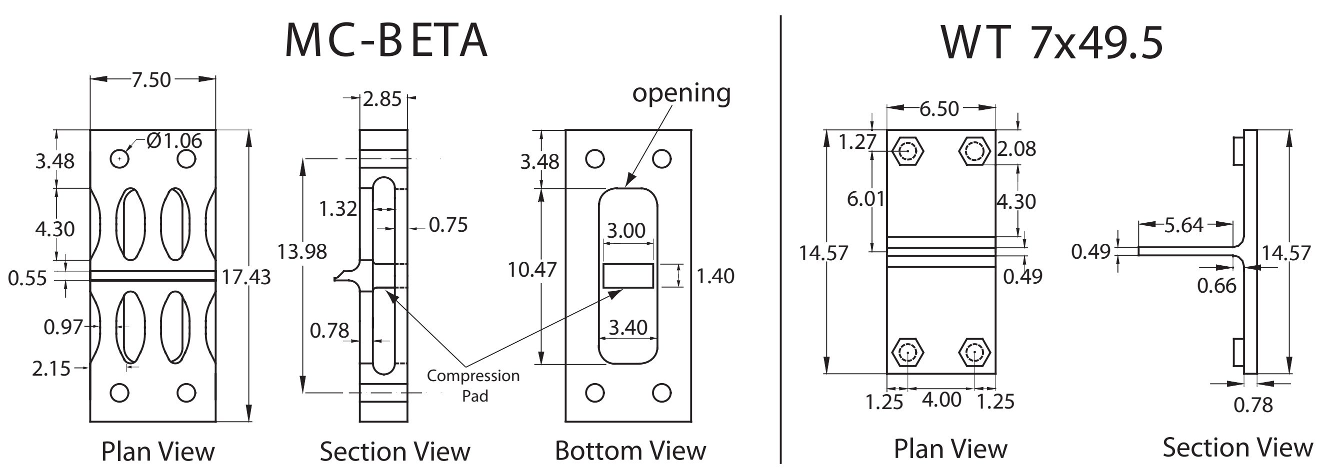

Fig. 6. Specimen dimensions: (a) scaled MC Beta prototype; (b) T-Stub (WT 7×49.5).

Table 4. Test Specimen Material Properties							
Test Specimen	Nominal		Actual				
	F_y, ksi	F_u, ksi	F_y, ksi	F_u, ksi	Elongation, %	Reduction, %	Brinell, Bhn
MC	40	71	39.8–43.0	61.0–67.6	32–33	62–65	137
WT	36–50[a]	58–65	63.7	77.0	32	76	–

[a] ASTM A36 was ordered (analyses used a F_y of 42 ksi); properties seem to imply Grade 50 steel.

gush and Soong, 1995) using a plasticity model possessing calibration parameters (Chaboche, 1989). This latter material model, termed "combined" in the text and "CHAB+MISO" in figures, seems a promising option as it will be shown to produce accurate global (load-deflection) and local (strain history) predictions under cyclic loadings. This model will be extended to evaluate the MC in a full-scale connection (see "Future Work").

Predicted Performance: MC versus WT

Figure 7 shows equivalent plastic strain contours of symmetry models of the scaled MC Beta and WT of similar strength and stiffness at identical deformation demand (0.05 radian for a W30 beam). These monotonic load comparisons use the MKIN model. As seen, the plasticity is spread throughout the arm for the MC and is concentrated for the WT (see table inset in Figure 7 for values). Further, significant yielding is observed in the WT bolts in the threads (due to the added axial force due to prying), and in the shank due to the combination of moment (from prying) and shear (due to catenary-action induced bolt bearing) as described in Sumer et al. (2007). Conversely, for the MC Beta, these forces are equilibrated in the base, leaving the bolt relatively unaffected. These monotonic results show that the arm elements and base end region virtually eliminate high plastic strain demand and bolt prying forces, and hence imply the potential for exceptional seismic performance of the MC Beta prototype in terms of ductility and reliability. This performance is directly verified in "Experimental Results: Monotonic Response." The experimental verification of the MC Beta prototype will additionally show a connector possessing exceptional energy dissipation, cyclic ductility characteristics, and overstrength characteristic (see "Experimental Results, Cyclic Response").

EXPERIMENTAL PROGRAM

The experimental program included: (1) verification of the monotonic behavior of the scaled MC Beta prototype with respect to the analytical predictions; (2) examination of the cyclic behavior of the scaled MC Beta prototype; and (3) direct comparisons of the scaled MC Beta prototype response to a WT section representing the detail from an analogous tee stub connection.

Test Specimens

Figure 8a shows the scaled MC Beta prototype after casting. Refer to Figure 6a for the compression pad detail that transmits beam flange compressive forces directly to the column

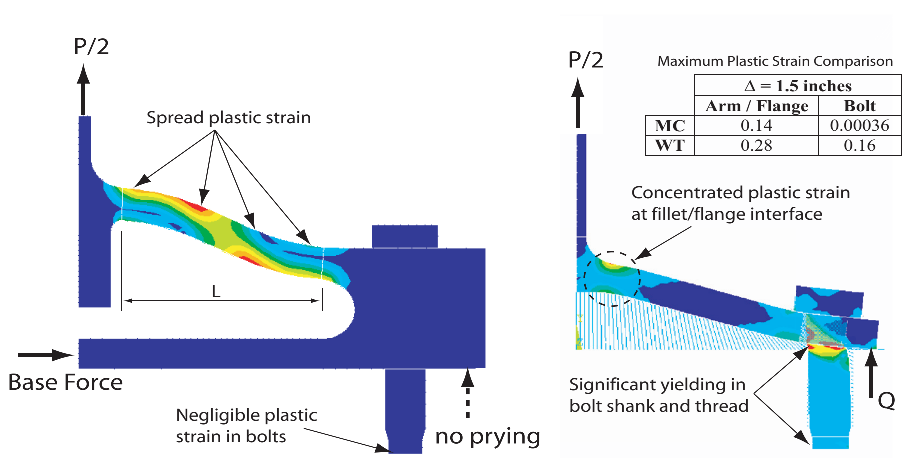

(a) (b)

Fig. 7. Expected performance from analysis (Sumer et al., 2007): (a) MC; (b) WT.

Table 5. Test Descriptions									
Test ID	**Type of Loading**	**Section**	**Bolt (4 bolts)**	ψ[b]	**Bolt Pretension kips**[e]	**Failure Location**	**Max. Stem Displacement in.**	P_y **kips**	P_u **kips**
MC-1	Monotonic	Casting	⅞ in. A325	1.11	37.2–37.4	Arm (C)[c]	2.55 in.	33.4	146
MC-2	FEMA 350	Casting	1 in. A325	–	51.7–52.1	Arm (C)[c]	1.90 in.	32.1	138
MC-3	Cyclic[a]	Casting	⅞ in. A325	–	37.1–39.1	Arm (B)[c]	44 cycles @ 0.72 in.	32.6	64.0
MC-4[d]	Monotonic	Casting	⅞ in. A325	–	38.3–39.9	Base	1.65 in.	32.0	125
MC-No Base-1	Monotonic	Casting	1⅛ in. A490	1.90	85.1–85.7	Arm (C)[c]	2.54 in.	36.7	177
MC-No Base-2	FEMA 350	Casting	1⅛ in. A490	–	80.1–86.9	Arm (B)[c]	2.31 in.	37.7	159
T-Stub-1A	Monotonic	WT7×49.5	⅞ in. A325	1.33	36.7–37.0	Bolt	1.90 in.	47.7	122
T-Stub-1B	Monotonic	WT7×49.5	1 in. A325	1.47	52.5–54.7	Bolt	1.90 in.	49.2	144
T-Stub-1C	Monotonic	WT7×49.5	1⅛ in. A490	1.83	83.4–86.8	Bolt	1.90 in.	49.7	184
T-Stub-2	Cyclic[a]	WT7×49.5	1⅛ in. A325	–	83.1–83.3	Flange	19 cycles @ 0.72 in.	48.0	82.0

[a] Constant amplitude cyclic = 0.72 in. represents 0.03 radian for a W24 beam.
[b] $\psi = (n_b \phi R_n)/P_u$, n_b refers to the number of bolts used in tests. In all tests 4 bolts are used (n_b = 4).
[c] MC arm failure location at B or C shown in Figure 10a.
[d] Distance between bolts changed from 13.98 in. to 15.85 in. to examine *e*/*s* ratio.
[e] Expressed as a range from the minimum to maximum pretension observed in the instrumented bolts. Minimum pretension is 39 kips for ⅞ in. A325, 51 kips for 1 in. A325, 80 kips for 1.125 in. A490 bolts (AISC, 2001).

during cyclic response. Figure 8b shows the "MC-NoBase," a MC cast without the base element. The MC-NoBase served as a control to directly evaluate the ability of the base to reduce prying forces. The WT specimen is shown in Figure 8c. The intent was to examine WTs of the same strength and stiffness as the scaled MC prototype. Though the nominal strengths matched, the actual yield stress of the WT was significantly higher than nominal (see Table 4). This condition, combined with the fact that the actual strength of a cast piece is generally slightly lower than the yield strength from the test bar due to variability in the casting process (Varicast, 2002), caused the test specimen strengths to not align. The yield strengths achieved in each test are indicated in Table 5 (in the column "P_y"). For this reason, certain plots have been normalized relative to each test's yield load to clearly show overstrength characteristics.

(a) (b) (c)

Fig. 8. Test Specimens: (a) scaled MC Beta prototype; (b) MC-No Base, and (c) WT 7×49.5.

Loading Protocol

The experiments are performed on isolated connectors under loading histories of direct axial tension/compression. This loading simulates the major force component in the beam flange due to beam moment, and ignores the beam shear; consistent with the analytical development of the MC Beta prototype design through evaluations of isolated connectors (Sumer et al., 2007) (refer to Figure 5). The approximations used in the isolated connector approach were shown to be acceptable for development of the MC form (Sumer, 2002). Once verified, the full scale MC Beta prototype will be evaluated in a full beam-to-column joint (see "Future Work").

The isolated connector tests were conducted under displacement control in a MTS 220 kip Hydraulic Testing Machine using a specially designed text fixture (see Figure 9a). Monotonic tests provide a reference backbone for evaluating cyclic results. The FEMA 350 testing protocol (FEMA, 2000) specified for full connections was modified [similar to loading protocol used by Swanson and Leon (2000)] to produce the axial cyclic load history for the isolated connector (see Figure 9b). This load protocol is based on the simple geometric transformation shown in Figure 5 for the 24-in.-deep beam as specified in "Scaled MC Beta Prototype". Constant amplitude (0.03 radian) cyclic test load histories are also performed using the same transformation. In cyclic tests, the compression cycle is performed under load control to achieve a compressive force equal to the maximum tension force achieved in the previous half-cycle. Test descriptions and key results are given in the test matrix appearing in Table 5.

Instrumentation

Figure 10a shows the strain gage layout along the MC arm elements. Strain gages were placed along the top and bottom

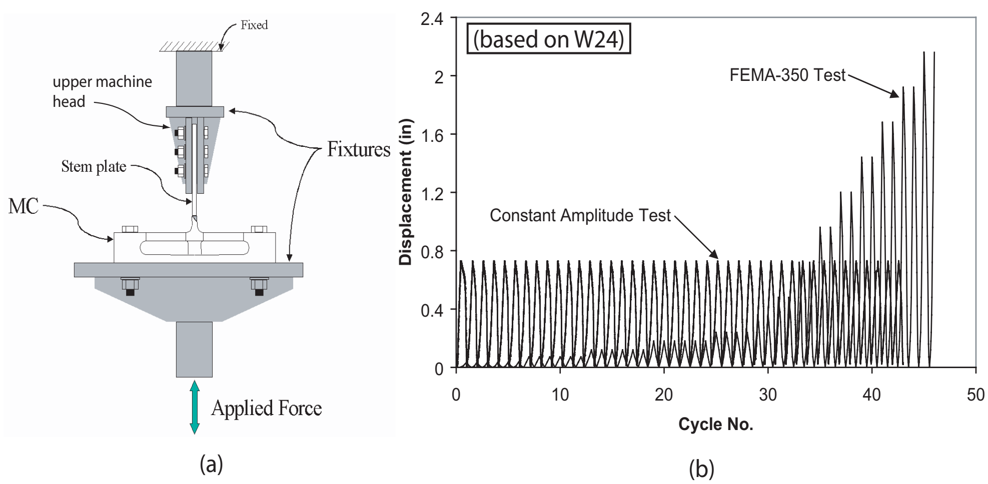

Fig. 9. Isolated testing: (a) fixture setup for direct pull tests; (b) loading protocol.

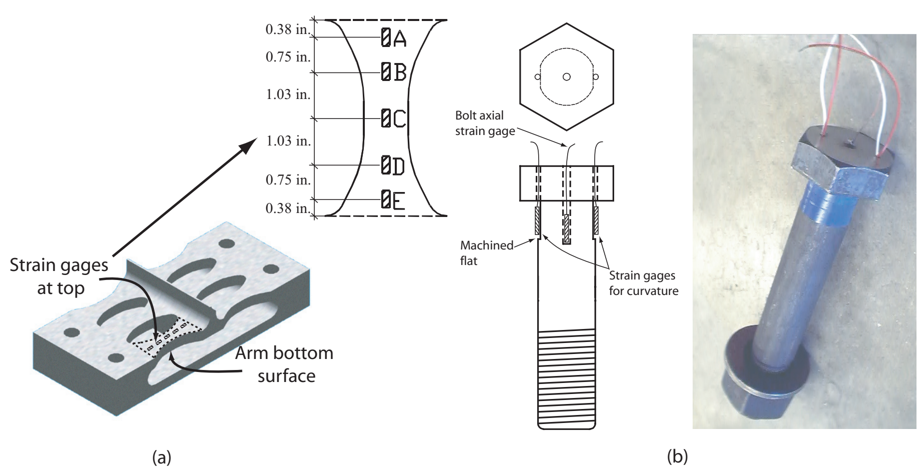

Fig. 10. Instrumentation: (a) strain gages on arm; (b) strain gages for the bolt.

surfaces of the arm. In most tests, these were ⅛-in.-long encapsulated gages; in one monotonic test (MC-1) and one cyclic test (MC-3) an array of 1⁄16-in.-long unencapsulated gages was used to monitor the strain distribution along the MC arm in higher resolution. Figure 10b shows the manner in which the bolts were instrumented. For the cases where the bolt shank remained elastic, bolt forces were calculated directly from the gages applied at the underside of the bolt head. For cases where the bolt shank yielded, bolt elongation measurements provided by linear variable displacement transducers (LVDTs) were used as an indirect measure of the bolt force (Kulak, Fisher, and Struik, 1987). LVDTs also provided measurement of bolt slip and bolt rotation.

The strain gages on the bolt shank were also used in the bolt-tightening procedure to assure meeting code-specified minimum pretensions (AISC, 2001). Initial pretensions were within 7% (see Table 5) of the code-specified minimum pretensions. In all cases, the bolts were tightened prior to the attachment to the clevises of the upper machine head (refer to Figure 9a). The data acquisition system read continuously through this process to ensure decompression or bolt overload did not occur.

EXPERIMENTAL RESULTS

In the following: (1) the monotonic behavior of the scaled MC Beta prototype is compared with respect to the analytical predictions and the WT; (2) the cyclic behavior of the scaled MC Beta prototype is compared with respect to the analytical predictions and the WT; (3) the performance of the scaled MC Beta prototype is examined under the FEMA 350 loading; and (4) the efficacy of the analytical models are evaluated. For convenience, the term "sMC Beta" will be used to refer to "scaled MC Beta prototype."

Monotonic Response

Figure 11a compares the load versus deflection of the sMC Beta and WTs in the monotonic tests, normalized to the same yield strength. The sMC Beta achieves a high monotonic ductility (0.10, 0.085 and 0.07 rad rotation for a 24-in.-, 30-in.-, and 36-in.-deep beam, respectively). The connection undergoes a "necking" failure as shown in Figure 11b. Throughout the test, the sMC Beta suffered no distress in its ⅞-in.-diameter ASTM A325 bolts; contrast this with WT tests in which all suffered bolt failures, including up to 1⅛-in.-diameter ASTM A490 bolts. Because of the different material strengths, it is important to compare the bolt strength relative to the connection capacity. This information is provided by the nondimensional parameter ψ given in Table 5. ψ expresses the design overstrength of the bolt relative to the connection. As seen, comparing tests MC-1 and T-Stub-1C, the bolt design overstrength for the sMC Beta is only 11% compared to 83% for the WT test; yet the MC bolts suffer no distress while the WT bolts fail.

Figure 12a shows good agreement in stability point (onset of "necking") predictions between finite element analysis and the experimental results. This outcome is useful in that the ability to analytically predict the stability point deflection (along with strength and stiffness) will facilitate subsequent development of a family of connectors. Figure 12b shows a strain versus deflection plot at three specific regions along the top of the arm (refer to Figure 10a for strain gage locations). The inset in Figure 12b shows a schematic of the deformed arm indicating that strain gages A, C, E are under: (A) axial tension + flexural tension; (C) axial tension only; and (E) axial tension + flexural compression. In each case, the axial tension is due to catenary force. Note the excellent agreement between the experiment and the analysis. It

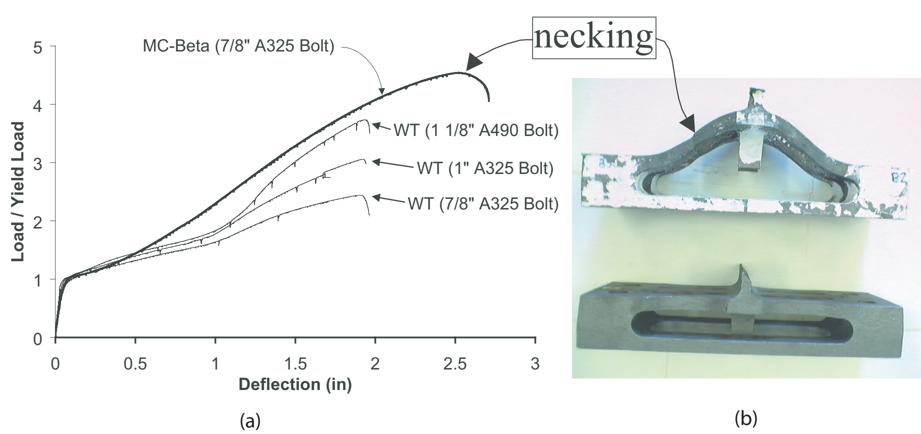

Fig. 11. (a) Load versus deflection; (b) MC Beta mechanism.

should be further noted that though the eventual monotonic failure is necking of the arm at C (due to the catenary force), no plastic strain demand occurs at this location until a deformation equivalent to a fairly significant beam rotation (approximately 0.03 radian for a 24-in.-deep beam, 0.025 radian for a 30-in.-deep beam). At this deformation demand, the maximum strain is seen instead to occur at region A. The delayed onset of straining at region C is due to the nonlinear nature of the catenary force, in other words, these forces are negligible at lower deformation demands. This feature has (positive) ramifications for the cyclic response of the MC, as described in the next section.

Figure 13a shows the bolt forces for three experiments using ⅞-in.-diameter ASTM A325 bolts: (a) test WT1; (b) test MC1, possessing bolt spacing that does not satisfy Equation 1; and (c) test MC4, possessing bolt spacing that satisfies Equation 1. As seen, the WT bolt forces (estimated here through bolt elongation data) indicate early prying. For test MC-1, even without consideration of optimum end region geometry, the MC base region is able to delay the prying and lower the prying forces (estimated through strain gage data). In test MC-4, possessing the optimum MC end region geometry, the bolt essentially has no prying force at all.

This plot does not fully show the extent of reduction in bolt demand provided by the MC as the WT bolt failure mode also involved catenary-force induced shear. A failed bolt from one of the WT tests is shown in Figure 13b alongside a plastic strain contour plot showing the finite element combined (axial/shear/flexure) failure mechanism prediction.

Cyclic Response (Constant Amplitude)

A difference exists in the MC monotonic and cyclic failure modes. For this reason, the monotonic test comparison shown in Figure 11a does not fully reveal the great advantage the MC possesses in low cycle fatigue life over a WT. In the previous section, the monotonic failure was seen to occur at the minimum area (region C of Figure 10a) and is a "necking" failure due to axial force created by catenary action. However, the results of Figure 12b also indicated that this region does not attract high strain until the MC achieves significant deformation. For the ductility demands expected in a design level seismic event [~0.025 radian (IBC, 2003)], the location of maximum straining will instead be at a flexure dominated region (A or E). Further examination of Figure 12a indicates that it will likely be region A, though under cyclic loading the behavior can be complex (see "Evaluation of Material Models"). Regardless, a different region is critical for the MC under cyclic load than for monotonic load, and this implies that the MC low cycle fatigue life under expected ductility demands may be far superior. Indeed, this outcome is evidenced in the number of survival cycles (44 versus 19) at constant amplitude (0.72 in.) in cyclic tests of the sMC Beta and WT (see Table 5). Note that simply to be able to make this comparison required a WT specimen with 1⅛-in.-diameter ASTM A490 bolts (in contrast to the ⅞-in.-diameter ASTM A325 bolts used in the sMC Beta specimen). The difference in failure mode between the monotonic and cyclic tests also explains why the accepted *cyclic* ductility requirement (AISC, 2005) was not used for the *monotonic* "useful range" during the MC development (Sumer et al., 2007).

In the cyclic constant amplitude test (MC-3), bolt forces are seen to decrease as the sMC Beta is cycled at levels that should keep the bolt elastic (see Figure 14). The reason for this decompression was believed to be relaxation of an initial camber (out-of-flat) of the MC base (see camber in Figure 14 inset). The average initial camber measurement prior to the

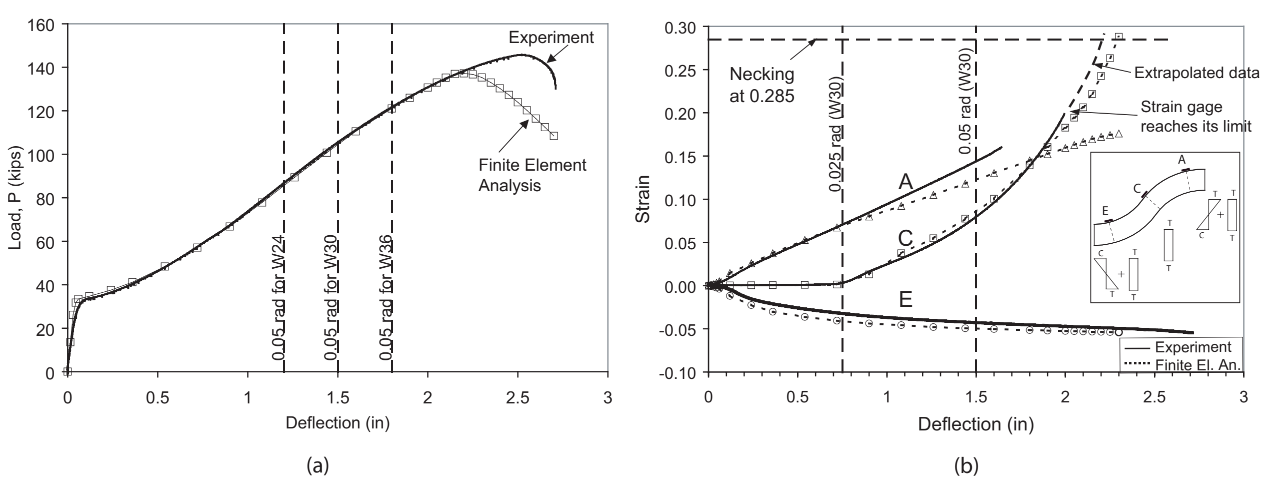

Fig. 12. (a) FE versus test: strain demand in MC Beta arm; (b) verification of critical strain.

test was 1/32 in. The post-test inspection measured final camber near zero. As seen in Figure 14, the effect of the camber on the bolt forces predicted by the finite element analysis is consistent with the experimental results. Accounting for the base camber also provides a more accurate prediction of the initial stiffness of the sMC Beta (see Figure 15). The quality control of this "camber" in the casting process is planned as a point of emphasis in the future casting of the full-scale MC Beta prototype.

FEMA 350 Loading

Figure 16 shows the load-deflection plot from Test MC-2, the FEMA 350 cyclic test. A distinct characteristic of the MC is the widening distance between the positive and negative yield surfaces as the cyclic amplitude increases (compare the distance between points II and VII with points III and V). This behavior occurs due to the plastic elongation of the arms under catenary forces. On load reversal, the arms are longer than their original dimension. Thus chord action develops in the arms until the load is sufficient to "snap-through" from concave to convex curvature (see progression of insets III, V, and VI in Figure 16). The chord action allows the unload reload path to become much greater than that associated with the Bauschinger effect. Essentially, while typical bolted connections will slip back along the column face into bearing, and then reverse the permanent set of the detail piece in flexure until it contacts the column, causing pinching of the overall moment-rotation hysteresis plot (Sims, 2000), the MC will resist the compressive force at or near the previous tension deflection. This behavior will be a point of focus in the future examination of the full beam-to-column connection.

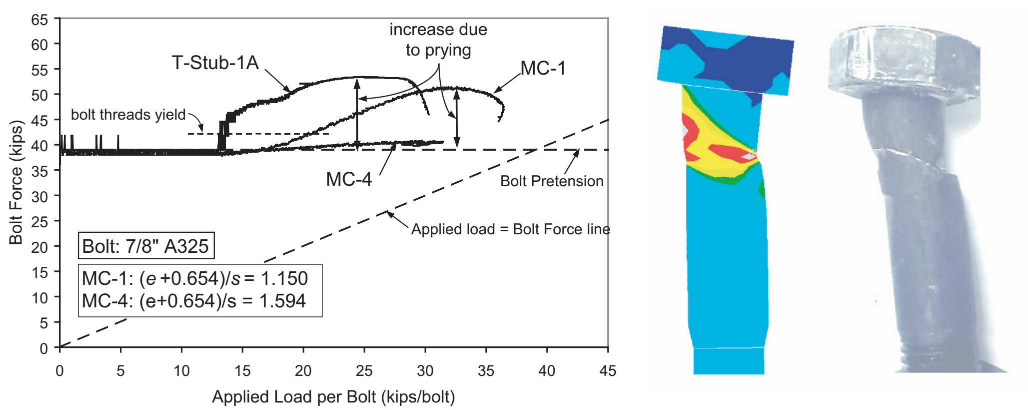

(a) (b)

Fig. 13. (a) Bolt axial forces in monotonic tests; (b) Failed bolt in WT.

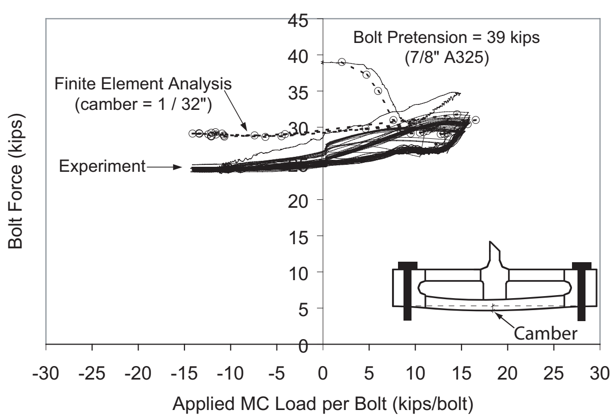

Fig. 14. Bolt axial forces in cyclic tests: constant amplitude test versus FE analysis.

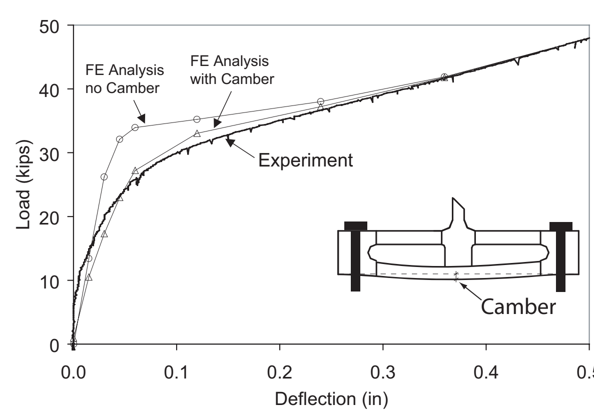

Fig. 15. Effect of camber on the MC global response.

The high compressive forces generated at the "snap-through" zone (point V in Figure 16) can lead to a torsional instability of the MC at high ductility demands (see Figure 17a). This behavior causes a slight loss of (compressive) load but more importantly amplifies the strain increment in high flexure regions (A or E) such that the ductility capacity can be reduced. To eliminate this deformation mode, guide plates were added as a retrofit to the MC Beta prototype (see Figure 18). The guide plates successfully eliminated the twisting mode by providing a bearing surface to align the compression pad. This detail can be included as a standard (cast) feature on subsequent MC prototypes.

The twisting mode had not been anticipated in cyclic analyses because of the MKIN hardening rule used in the finite element model (see "Evaluation of Material Models"). This behavior was however captured when the combined material model was used. An initial imperfection must be introduced into the finite element model of an isolated connector to produce the torsional instability mode (in a real connection this would be present naturally or induced by beam shear). This initial imperfection was applied as an initial displacement field using the mode shape from an elastic eigenvalue buckling analysis scaled to a maximum amplitude of 0.03 in. based on casting tolerances (Sumer, 2002). A nonlinear

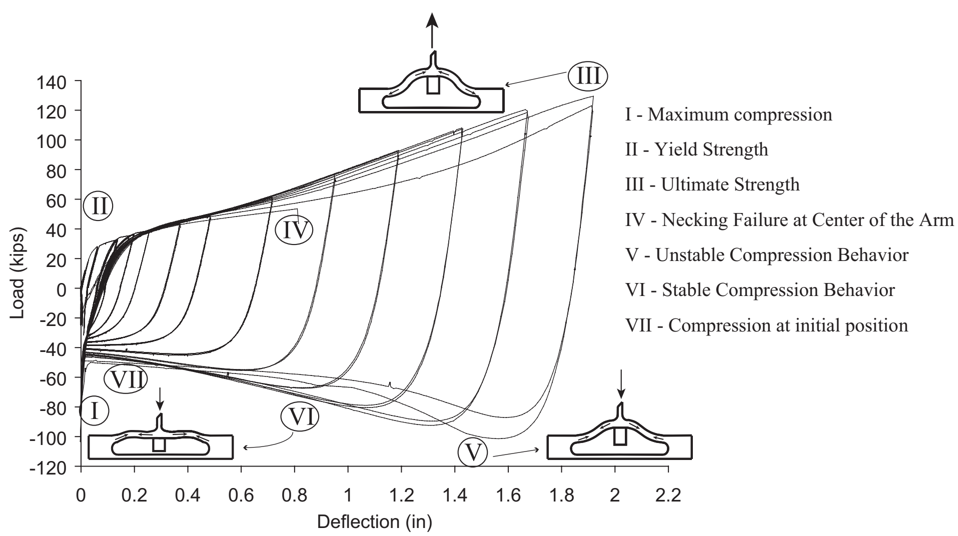

Fig. 16. Beta prototype under FEMA 350 loading.

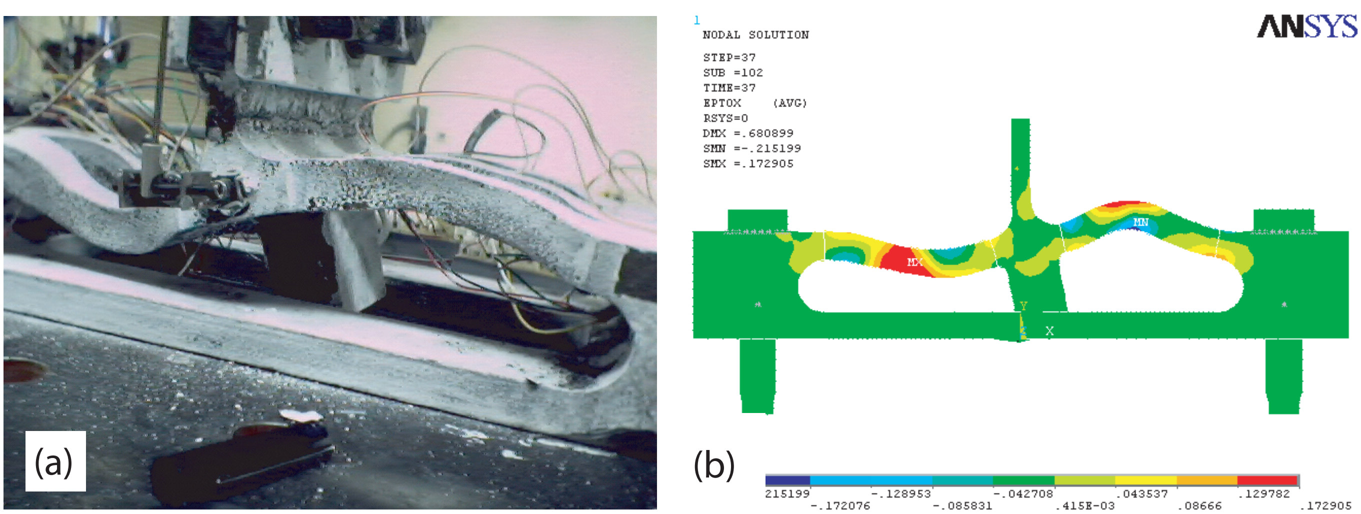

Fig. 17. (a) Torsional instability mode; (b) Strain contour plot.

cyclic analysis with the imperfection introduced successfully simulated the torsional instability mode at load reversals (see Figure 17b).

Evaluation of Material Models

The MKIN material model accurately predicted monotonic response (for example, Figures 12, 13, and 15). Examination of Figure 19a, however, shows that the MKIN model is unable to track the widening of the hysteresis curves in the cyclic analysis. This condition stems from the inability of the MKIN model to capture the second order effects associated with arm elongation that causes the widening phenomenon. For this reason, the MKIN model was also unable to predict the torsional instability described in the previous section.

The isotropic hardening model (MISO) accounts for second order effects and thus captures the hysteresis widening (also shown in Figure 19a), but is seen to overestimate strength at lower deformation demands and underestimate strength at large deformation demands (see Ricles, Fisher, Lu, and Kaufmann, 2002). The combined material model, on the other hand, provides sufficiently accurate global response (load-deflection) under monotonic and cyclic loadings (see Figure 19b). Likewise for local behavior, the combined model is seen to provide the best prediction of cyclic plastic strains in terms of magnitude (Figure 20a) and accumulation (see Figure 20b) for the FEMA 350 tests. A similar conclusion can be drawn from constant amplitude test MC-3 (see Figure 20c).

The importance of accurate cyclic plastic strain modeling is evidenced in the evolution of damage in the MC arm. Figure 21 shows the progression of plastic strain contours of the MC arm from a simulation of cyclic test MC-3 using the combined material model. The arms on the left are at the maximum deflection; the arms on the right are at zero deflection. Instantaneous maximum plastic normal strain (along the arm) is plotted. A well-defined elastic-plastic interface develops in the first cycle and is essentially reversed on the first compression cycle. However, as the MC arms are additionally cycled, the plastic zone continually migrates. After a number of cycles, there are portions of the arm in the *tension* region that are under net *compressive* plastic strain and vice versa. This behavior was confirmed in the strain gage data and enhances the low cycle fatigue life as no single fiber is continuously damaged at a critical location. The combined material model is able to capture this complex phenomenon and also accurately predict the failure location in the arm (see photo inset of Figure 21).

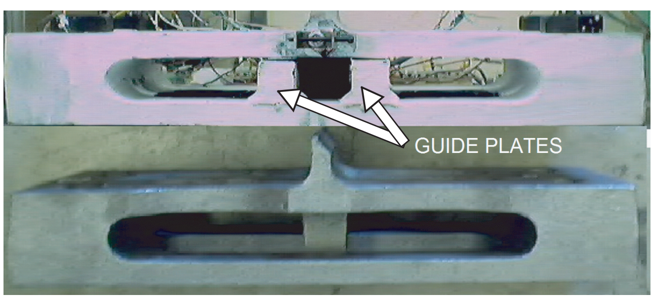

Fig. 18. Retrofitted and unretrofitted MC.

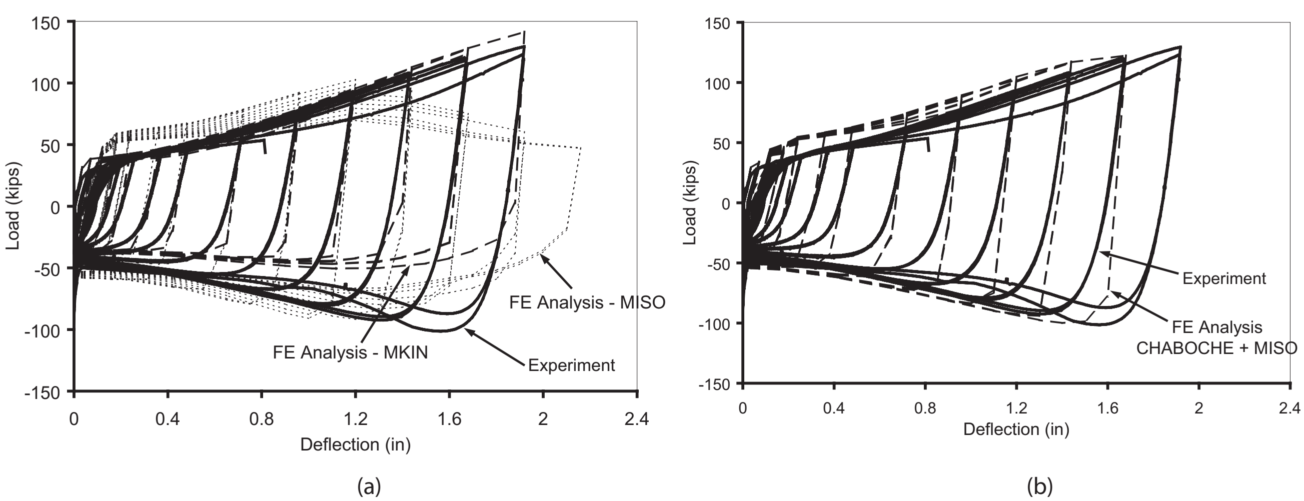

Fig. 19. Global cyclic response: (a) using MKIN model, using MISO model; (b) combined model.

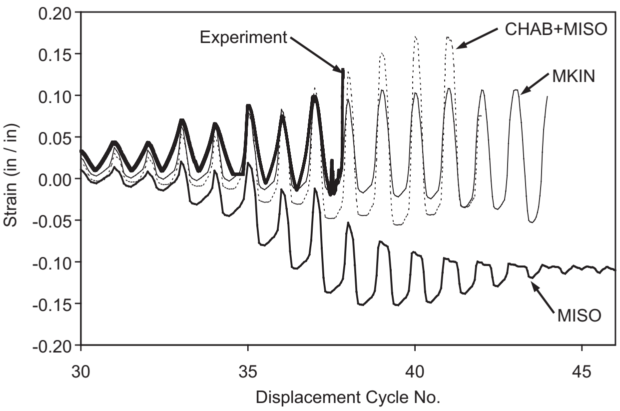

(a)

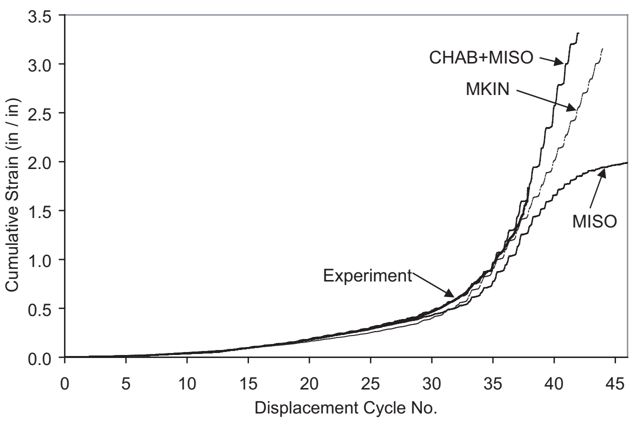

(b)

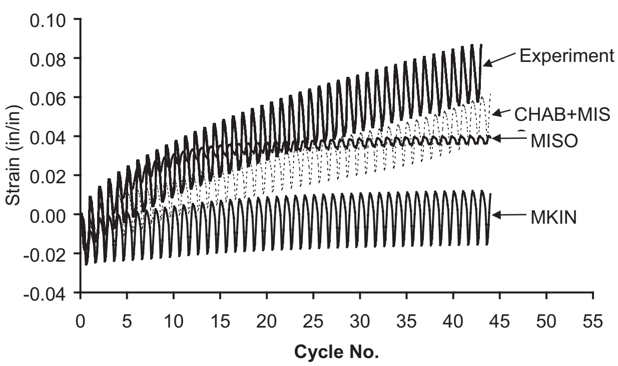

(c)

Fig. 20. Strain comparison: (a) location B, MC-2; (b) cumulative strain at location B, MC-2; (c) location D, MC-3.

FUTURE WORK

The MC Beta configuration has been analytically developed and experimentally verified as a viable cast connector through evaluation of the isolated connector. The focus will shift in the next phase to the beam-to-column connection as a whole. Subsequent steps in the development of an implementable MC are: (1) Examination of the full beam-to-column connection; (2) Evaluation of frame performance; and, (3) Development of design guidelines for a family of MCs. Some aspects of the transition from a focus on the isolated MC connector to the future work on full connections are briefly discussed here.

MC Beam-to-Column Connection

The MC beam-to-column connection involves MCs at the flanges for moment transfer and a web connection for the beam that participates in transferring large seismic shears from the beam to column. The connection classification will likely be semi-rigid and it is envisioned that the MCs will be used throughout the structure, rather than in a few isolated frames.

The response of the MC in a full connection will be affected by several conditions that are not fully captured in the isolated connector approach used to develop the MC prototype configuration. These conditions include: (1) a trajectory that is not direct axial displacement but also contains transverse and rotational degrees-of-freedom that modify the strain distribution; (2) the associated shears and moments that develop at the MC stem which are determined by the indeterminate system of the top and bottom connectors and web connection; forces that can impact the capacity design of both the column face bolts and the MC stem-to-beam flange weld; (3) a cyclic history that is determined in part by the instantaneous stiffness of the elements in the system and the contact condition of the MC under compression and can include arm instability modes if not mitigated. The MC Beta prototype will be extended to a "Beta-2" prototype to better accommodate these conditions.

Beta-2 Prototype

The Beta-2 prototype will be an enhanced version of the MC Beta prototype described in this paper, and will incorporate features better suited to interface with the beam, maintain cyclic stability and handle the indeterminate force condition (shear and local bending actions) at the beam end. A candidate for the Beta-2 prototype is shown in Figure 22. Added features may include: (1) a web tab that provides leverage to significantly reduce local bending on the beam flange full penetration weld under combined beam flange tension and shear, thus keeping it elastic throughout the response; and (2) a second set of arms in the base (parallel to the base) that has shown promise to both lessen the effects of the beam shear on the arms (in other words, lower the unbalance in plastic strains due to a shear force in addition to the tension force) and mitigate the torsional instability described in the previous section. Thus, this detail may replace the guide plates in future versions of the MC. It should also be noted that on the basis of discussions with the AISC industry partners, a completely bolted version of the Beta-2 prototype is also under investigation. The exact form of the Beta-2 prototype will be determined in the next phase of the research.

The Beta-2 prototype will be evaluated through finite element analyses of the MC beam-to-column connection including a web connection. Relationships between connector geometry and connection strength and stiffness will be established. Once finalized, this prototype will be verified through full-scale experiments in accordance with accepted qualification protocols (AISC, 2005).

Guidelines for the Design of MCs

The final stage will be to develop design guidelines for a family of modular connectors. The performance of the partially-restrained (PR) frame with MCs will be evaluated to determine appropriate force reduction (*R*) and overstrength (Ω_0) factors for seismic design of buildings. Design procedures will be developed to make the appropriate selection of members and MCs.

The guidelines will be based on a limited number of MCs that cover a reasonable design range. For instance, a single MC size with a beam interface detail able to accommodate welding to a limited range of compatible flange thickness values has possible widespread use throughout the structure if the floor-by-floor change in beam depth reasonably matches the change in seismic forces, as is often the case. In

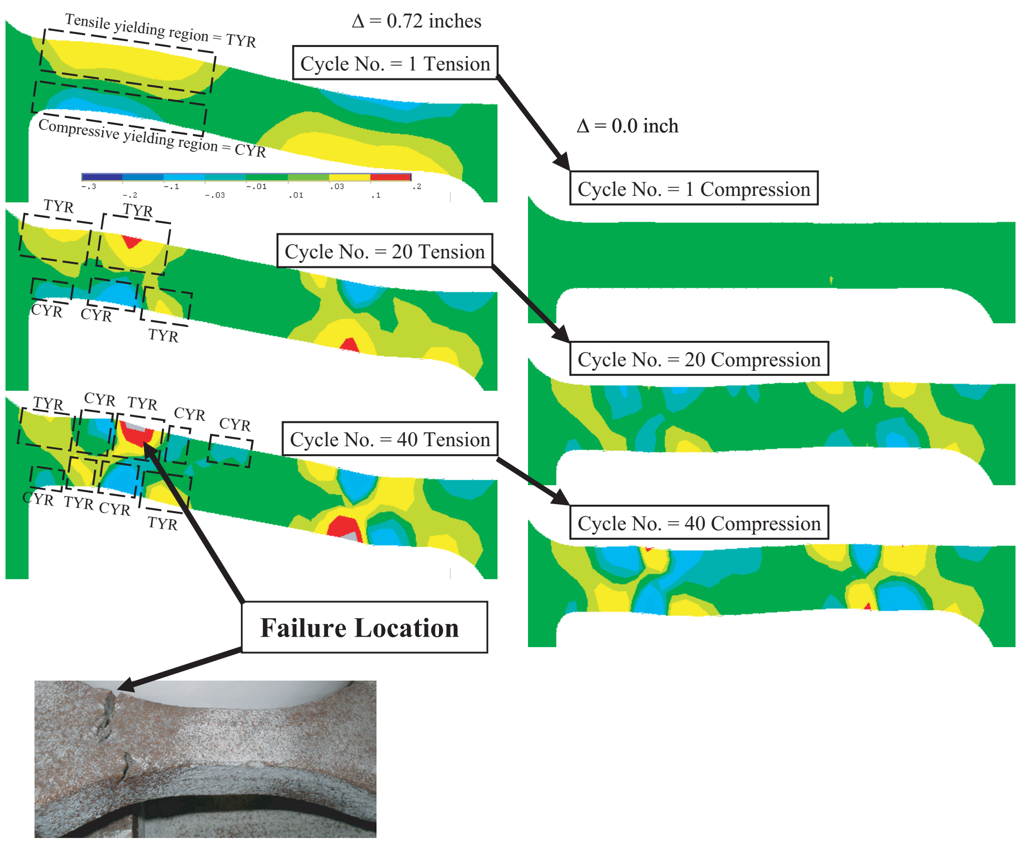

Fig. 21. Constant amplitude loading: plastic zone migration.

this way, a MC of a single (axial) strength and stiffness will create beam-to-column moment connections with increasing rotational strength (proportional to d_{bm}) and stiffness (proportional to d^2_{bm}) required to meet the (typically drift-controlled) design (refer to Figure 5).

CONCLUSIONS

A bolted cast modular connector, the MC, has been conceived, developed, and prototyped. The MC (Beta) prototype was tested in isolated fashion at approximately half-scale. The MC Beta has shown great promise for using castings as special energy-dissipating details in steel moment frames in high seismic zones by exhibiting:

- Superior ductility with respect to traditional connections
- Stable and efficient energy dissipation
- Increasing strength under large strains due to catenary action
- Reliability and repeatability

The excellent performance of the MC Beta is a product of two features easily cast:

- Variable section arms that spread the plastic zone thus eliminating strain concentrations.

  These arms produce outstanding ductility and exhibit a hysteretic characteristic free from degradation or slip.

- A stiff end-region connected by a base that eliminates prying and shear force on the bolts.

  This feature permits the MC arms to be sufficiently long to produce outstanding ductility without a concern for bolt failure. In fact, the bolts in an MC connection can be designed simply for the maximum possible direct tension.

The MC Beta is currently being extended to a Beta-2 Prototype for use in analytical and experimental evaluation of the full beam-to-column connection. Once established, a design procedure is planned for a family of MCs.

ACKNOWLEDGMENTS

This research was supported by NSF CAREER Award Grant CMS-01-96120. Supplemental funds were provided by AISC and SFSA. Industry partners Varicast, Inc. and Able Steel created the prototype specimens. The reaction frame was provided through a donation by ConXtech, Inc.; the computer laboratory through a grant from Intel, Inc.; and the finite element software was donated by industry partner Swanson, Inc. (ANSYS). The authors are grateful for this support.

Any opinions, findings, and conclusions or recommendations expressed in this material are those of the author(s) and do not necessarily reflect the views of the National Science Foundation.

NOMENCLATURE

B_{max} = maximum width of MC arm

B_{min} = minimum width of MC arm

d_{bm} = depth of beam

e = distance between center of bolt and MC arm

e_0 = distance between center of bolt to end

F_y = yield stress

F_u = ultimate stress

F.O.S. = factor of safety

K_i = initial stiffness of entire MC Beta

K_{rot} = rotational stiffness of entire MC Beta

L = length of MC arm

L_{bcl} = base element length

n = number of MC arms

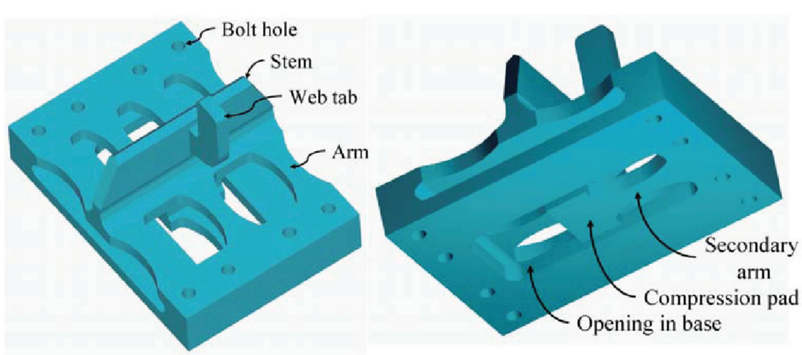

Fig. 22. Candidate for Beta-2 modular connector—isometric views.

n_b = number of bolts in modular connector

P = beam flange force tributary to entire modular connector

P_y = yield load of entire modular connector

P_u = ultimate load of entire modular connector

$P_{0.05}$ = load of entire modular connector at 0.05 radian connection rotation

Q = prying force

R_n = nominal tensile bolt strength

s = distance between MC arm and MC base (from center-to-center)

s_0 = clear distance between MC arm and MC base

t, t_b = MC arm thickness, base thickness

w_b = base element width

W_{MC} = MC width

W_0 = base opening width

Δ = MC arm transverse displacement

Δ_y = MC arm transverse displacement at yield point

Δ_u = stability point

$\Delta_{0.05}$ = useful limit

θ_{conn} = beam end relative rotation

ϕ = resistance factor

ψ = $(n_b \phi R_n)/P_u$

REFERENCES

AISC (2001), *Load and Resistance Factor Design Manual of Steel Construction*, American Institute of Steel Construction, Inc., 3rd ed.

AISC (2005), *Seismic Provisions for Structural Steel Buildings*, Appendix S, Chicago, IL.

American Society for Testing and Materials (2003), "Standard Specification for Steel Castings, Carbon, and Alloy, Chemical Requirements Similar to Standard Wrought Grades," ASTM Standard A915/A915M-03, ASTM International, West Conshohocken, PA.

ASTM (2004), "Standard Specification for Castings, Steel and Alloy, Common Requirements, for General Industrial Use," ASTM Standard A781/A781M-04a, ASTM International, West Conshohocken, PA.

ANSYS (2003), "Elements and Theory Reference," Version 8.0, 9th ed., SAS IP, Inc.

Chaboche, J.L. (1989), "Constitutive Equations for Cyclic Plasticity and Cyclic Viscoplasticity," *International Journal of Plasticity*, Vol. 5, pp. 247–302.

Dargush, G.F. and Soong, T.T. (1995), "Behavior of Metallic Plate Dampers in Seismic Passive Energy Dissipation Systems," *Earthquake Spectra*, Vol. 11, No. 4, p. 545.

Eagle Alloy (2000), "Steel Casting Mechanical Testing Reports," and transmittal.

FEMA (2000), "Recommended Seismic Design Criteria for New Steel Moment-Frame Buildings," FEMA 350, prepared by the SAC Joint Venture for the Federal Emergency Management Agency, Washington, DC.

Fleischman, R.B. and Sumer, A. (2006), "Optimum Arm Geometry for Ductile Modular Connectors," *Journal of Structural Engineering*, ASCE, Vol. 132, No. 5, pp. 705–716.

ICC (2003), *International Building Code*, International Code Council, Falls Church, VA.

Kulak, G.L., Fisher, J.W., and Struik, J.H.A. (1987), *Guide to Design Criteria for Bolted and Riveted Joints*, 2nd ed., John Wiley & Sons, Inc.

Ricles, J.M., Fisher, J.W., Lu, Le-Wu, and Kaufmann, E.J. (2002), "Development of Improved Welded Moment Connections for Earthquake-resistant Design," *Journal of Constructional Steel Research*, No. 58, pp. 565–604.

Sims, J.K. (2000), "Flange Behavior in Semi-Rigid Connections for Steel PR Frames," MS thesis, Department of Civil Engineering and Geological Sciences, Notre Dame, IN.

SFSA (1995), *Steel Castings Handbook*, 6th ed., Steel Founders' Society of America, ASM International, Materials Park, OH.

Sumer, A. (2002), "Development of Modular Connectors for Seismic Resistant Steel Frames," MS Thesis, Civil Engineering and Engineering Mechanics, University of Arizona, Tucson, AZ.

Sumer, A., Fleischman, R.B., and Hoskisson, B.E. (2007), "Development of a Cast Modular Connector for Seismic-Resistant Steel Frames, Part 1: Prototype Development," *Engineering Journal*, AISC, Vol. 44, No. 3, pp. 195–211.

Swanson, J.A. and Leon, R.T. (2000), "Bolted Steel Connections: Tests on T-Stub Components," *Journal of Structural Engineering*, ASCE, Vol. 126, No. 1, pp. 50-56.

Varicast (2002), "Steel Casting Mechanical Testing Reports," and transmittal.